CHINESE OPTICS LETTERS

Vol. 19, No. 10 | October 2021

Reconstitution of optical orbital angular momentum through strong scattering media via feedback-based wavefront shaping method

Lanting Li (李兰婷)[1], Yuanlin Zheng (郑远林)[1,2], Haigang Liu (刘海港)[1*], and Xianfeng Chen (陈险峰)[1,2,3,4**]

[1] State Key Laboratory of Advanced Optical Communication Systems and Networks, School of Physics and Astronomy, Shanghai Jiao Tong University, Shanghai 200240, China

[2] Shanghai Research Center for Quantum Sciences, Shanghai 201315, China

[3] Jinan Institute of Quantum Technology, Jinan 250101, China

[4] Collaborative Innovation Center of Light Manipulations and Applications, Shandong Normal University, Jinan 250358, China

*Corresponding author: liuhaigang@sjtu.edu.cn

**Corresponding author: xfchen@sjtu.edu.cn

Received February 13, 2021 | Accepted March 18, 2021

Orbital angular momentum (OAM) is a fundamental physical characteristic to describe laser fields with a spiral phase structure. Vortex beams carrying OAMs have attracted more and more attention in recent years. However, the wavefront of OAM light would be destroyed when it passes through scattering media. Here, based on the feedback-based wavefront shaping method, we reconstitute OAM wavefronts behind strong scattering media. The intensity of light with desired OAM states is enhanced to 150 times. This study provides a method to manipulate OAMs of scattered light and is of great significance for OAM optical communication and imaging to overcome complex environment interference.

Keywords: orbital angular momentum; scattering; wavefront shaping.

DOI: 10.3788/COL202119.100101

1. Introduction

Since 1992, the vortex beam has been proved to possess orbital angular momentum (OAM)[1]. The phase factor $\varphi(r,\varphi) = \exp(i\ell\varphi)$ can be used to describe the helical wavefront of such a vortex beam, where φ is the azimuthal angle, and ℓ indicates the topological charge, which can be any integer or fraction. Thus, the OAM of each photon is $\ell\hbar$, of which the number and direction of spiral phase planes depends on the value of the topological charge ℓ. Such vortex beams with OAM have donut shapes at the cross section of the light beam, which can be generated by spiral phase plates (SPP)[2], forked diffraction gratings[3], cylindrical lenses[4], and computer generated holograms[5]. Also, detection of such OAM beams can be performed with similar devices. The phase modulation or diffraction element with opposite topological charges can untwist the vortex light into a Gaussian beam, which can be detected experimentally by far-field diffraction[4]. In addition, more methods for accurately detecting OAM have been proposed recently, such as thermally tuned q-plates[6], diffraction patterns behind apertures[7], and transforming OAM states into transverse momentum states[8]. In the past few years, such a vortex beam has been widely applied to a variety of fields. It has been demonstrated that by using OAM beams as information carriers[9–11] the fiber and state also can provide a unique gradient force distribution, which has significant applications in optical tweezers[12] and light–particle interaction[13–15]. Light with OAM is also widely studied in quantum optics. For example, through parametric down conversion, OAM beams can produce multi-dimensional entangled states, which could be of considerable importance in the field of quantum information[16]. Moreover, it is also advantageous to improve the security and information capacity of quantum key distribution[17]. Meanwhile, due to the special optical vortices mode and spatial degrees of freedom, OAM beams also play important roles in other applications, such as super-resolution imaging[18], optical measurements[19], and high-precision measurement in quantum metrology[20].

However, scattering is always a fundamental limit in optical applications. A beam of coherent light incident into a turbid medium will be scattered and produce the speckle of random intensity. Over the past few years, the propagation and penetration properties of optical vortex beams in a turbid media have been investigated[21–23]. Although a higher transmittance of vortex Laguerre–Gaussian beams is demonstrated in the diffusive

region than the Gaussian beam[24], the helical wavefront will still be distorted when it passes through a strongly scattering environment, which will significantly influence its further applications in all kinds of fields. Therefore, a method to extract and reconstitute specific OAM information of scattered light is of great importance. In recent years, there have been some studies on spatial sorting[25], vortex mode analyzing[26,27], and demultiplexing[28] of scattered OAM beams.

The feedback-based wavefront shaping (FBWS) method was proposed by Vellekoop in 2007[29,30]. Although most quantitative descriptions of the light evolution process in a strong scatting environment is approximated, this process can be taken as a deterministic linear system if the scattering medium is static. Then, by shaping the incident wavefront correctly, the outgoing light can be focused or manipulated to any desired wavefront. The transmission matrix is an effective method to describe and manipulate scattered beams[31]. In 2012, Conkey and coworkers applied the genetic algorithm to wavefront optimization and proved that it was particularly advantageous in low signal-to-noise environments[32]. Ideally, it will finally achieve the local optimal solution, as long as an appropriate objective function for optimization is determined, with sufficient iteration. Besides, this technology has also been widely used in nonlinear harmonics focusing[33], glare reduction[34], spatiotemporal coherent control[35], non-invasive imaging[36,37], and deep focusing and imaging[38,39].

In this Letter, assisted by the FBWS method, we restore the OAM information of light behind strong scattering media. By using an SPP with an opposite topological charge as a detection component, the objective intensity steadily increases and approaches the local optimum with the operation of the genetic evolution algorithm. The enhancement factor is estimated to be 150 over 500 generations of the evolution. These experimental results are repeatable and suitable for OAM recovery of different topological charges. In addition, the reconstitution of OAMs around different optical axes is also demonstrated in our experiment.

2. Experiment

The concept of reconstituting optical OAMs via the FBWS method is shown in Fig. 1. Without wavefront shaping, the light behind the scattered material is mutilated as disordered speckles on the screen, as shown in Fig. 1(a). According to Huygens' principle, each point of the original spiral wavefront emits a wavelet. The optical pattern is the result of propagation and coherent superposition of every wavelet. When going through the strong scattering medium, each wavelet gets a random additional phase (as well as attenuation), which leads to the generation of the disordered speckle pattern. Such OAM states of light can be reconstituted forwardly by using a wavefront optimization procedure after the strong scattering media, as shown in Fig. 1(b). In the reconstruction processes, the SPP with opposite topological charge is used to detect the relative intensity of light carrying the specific OAM[40,41].

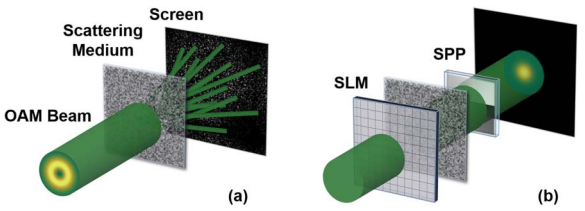

Fig. 1. Sketch map of optical OAM reconstitution through scattering media. (a) Without wavefront shaping, the OAM beam forms a disordered speckle pattern behind the scattering medium. (b) With an appropriate SLM phase mask applied in advance, optical OAM is reconstituted after scattering. Using an SPP with an opposite topological charge as a detection component, a focal point can be generated on the screen.

The experimental setup is illustrated in Fig. 2. A continuous wave (CW) laser at the wavelength of 532 nm is used as the light source. A half-wave plate (HWP) and a polarizer (P_1) after the laser are used to adjust the intensity and polarization of the incident light. Then L_1 ($f_1 = 30$ mm) and L_2 ($f_2 = 200$ mm) is a pair of beam expander lenses to allow the cross section of the laser beam to cover the modulation area of the spatial light modulator (SLM) as much as possible. The phase-only SLM (UPOLabs, HDSLM80R) is sensitive to horizontal polarization light and has a resolution of 1920 × 1200 pixels, each with a rectangular area of 8 μm × 8 μm. Each pixel can be independently controlled and converts the phase of light from 0 to 2π. Lenses L_3 and L_4 ($f_3 = f_4 = 200$ mm) constitute a 4-f imaging system. The SLM and SPP are, respectively, at the front and back focal plane of the 4-f system, which maps the phase modulation of the SLM onto the SPP to realize OAM detection. The scattering sample that we used here is TiO_2 powder, which is deposited onto an indium tin oxide (ITO)-coated glass substrate by the electrophoresis method. The TiO_2 powder layer is about 100 μm thick, and the transport mean free path is less than 10 μm, measured by the coherent backscattering method[42,43]. The inset in the bottom right corner of Fig. 2 shows the morphology image of the TiO_2 powder by using scanning electron microscopy. Lens L_5

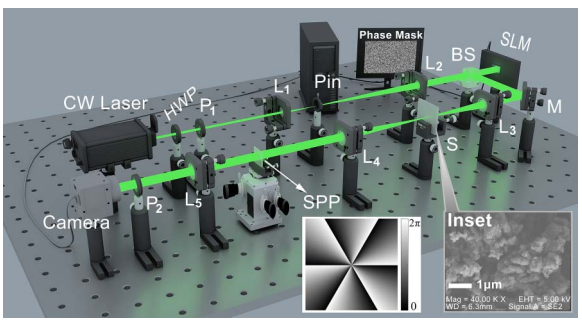

Fig. 2. Experimental setup for OAM restoration behind the strong scattering media. HWP, half-wavelength plate; P_1, P_2, linear polarizer; BS, beam splitter; SLM, spatial light modulator; M, reflecting mirror; SPP, spiral phase plates, which has a center-symmetrical phase distribution as shown; L_{1-5}, lens; f_{1-5}, 200, 200, 200, 100 mm. Inset: a scanning electron microscopy image of the TiO_2 powder.

is a Fourier lens ($f_5 = 100$ mm), which allows us to observe the far-field diffraction pattern, which is detected by a complementary metal–oxide–semiconductor (CMOS) camera (DAHENG IMAGING, MER-U3) at the Fourier spectrum plane. The CMOS camera has a resolution of 1280×1024 pixels, each with a rectangular area of $4.8\,\mu\text{m} \times 4.8\,\mu\text{m}$. A wave plate analyzer P_2 is placed before the detector to ensure polarization consistency after scattering. The pixels on the SLM are divided into square segments with side length of eight pixels, each of which serves as an independent modulation unit during the optimization. The genetic algorithm is written based on the Labview platform in order to control the hardware more conveniently. This process is mainly divided into three stages: initializing the population, sorting and screening parents, and crossing and mutation. To start with, a population of $N = 100$ phase masks is generated randomly as the first generation. Next, all of these masks should be ranked according to the objective function, which is defined by the intensity at the target region. One would have a higher chance to be chosen as a parental mask to breed the next generation. The genetic process is repeated until a desired pattern or a locally optimal solution is achieved[32].

Before algorithm optimization, it is important to set a suitable objective function for iteration. As mentioned above, the detection system is formed by an SPP, a far-field diffractive lens, and a CMOS camera, which forms the Fourier transform relationship in the plane of these three optical components. Firstly, the system is calibrated without the scattering medium. Figure 3 shows an experimental demonstration of measuring optical OAM. The intensity graph in Fig. 3(a) is the OAM state with $\ell = 6$ generated by the SLM, which is the goal of subsequent experimental restoration. Figures 3(b)–3(f) show the far-field diffraction patterns when such an OAM state with $\ell = 6$, respectively, passes through the SPP with the integer topological charges from $\ell = -4$ to $\ell = -8$. It is obvious and also demonstrated in previous researches that only if the topological charges of the OAM beam and SPP are just matching ($\ell_{\text{OAM}} = -\ell_{\text{SPP}}$), the dark hole in the center of the beam will transfer into a spot. Therefore, the relative intensity in this bright spot position can quantitatively reflect the light intensity of the OAM state that is coaxial with the SPP. The calibration process is to determine the position of the center bright spot during the far-field measurement. Secondly, we keep the entire light path unchanged in subsequent experiments, and the light intensity of such a bright spot area on the optical axis of the SPP is set as the objective function in our experiment.

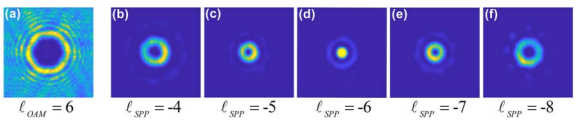

Fig. 3. Experimental demonstration of measuring OAM and calibration. (a) An example for the OAM state with $\ell = 6$ generated by SLM. (b)–(f) The far-field diffraction patterns while the OAM beam in (a) passes through an SPP with different topological charges.

3. Results

The complete reconstitution process of an OAM state of $6\hbar$ is revealed in Figs. 4(a)–4(c). After calibrating with an ideal OAM state, a circular area with a radius of 10 pixels is recorded by CCD and shown in Fig. 4(a). Next, we place the strongly scattering medium into the optical path and choose the same coordinates of the area shown in Fig. 4(b) as our target location to start the genetic algorithm optimization. The relative light intensity of the target area continues to increase, and finally a high-contrast spot is obtained, as shown in Fig. 4(c). The optimized results can be maintained for quite a long time, as long as the system does not receive artificial interference, which confirms that our system has great stability. The enhancement factor η is defined to quantify the optimization process, which is the ratio of the intensity at the detective region after optimization and the mean intensity of the scattering background. As expected, η increased generally with the generation number, and it can reach the value of 150 after around 500 generations in our experiment. As mentioned, the SPP can be regarded as a spatial filter, thus the zero-order component is selected at the Fourier spectrum plane to be the algorithm feedback. Though the data shown here has not completely converged, the overall enhancement has gradually slowed down, which is consistent with the convergence trend of the enhancement curve. A series of typical enhancement curves of different OAM states is also shown in Fig. 5(a). In this optimization process, the convergence speed has weak dependence on the OAM state to be restored. This is because the high disorder degree of the strong scattering medium completely disrupts the wavefront structure of the OAM beams. Therefore, the convergence speed is mainly affected by the hardware and algorithm programs we used. Figure 5(b) shows the result of measuring the stability over 10 h. The relative intensity of the focus only has a small decrease to around 94%, which indicates a good stability of the whole system.

As we know, the definition of OAM of light is determined by the direction of the optical axis. Besides, the manipulation of OAM at different directions also brings flexibility when it is used in different circumstances. Therefore, based on the same system, we also restore the OAM of light at different spatial directions in our experiment. By adjusting the angle of the reflect mirror after

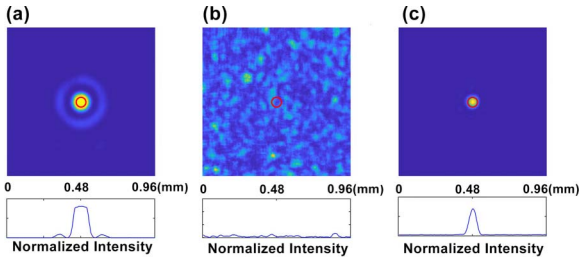

Fig. 4. (a) Calibration of detecting system with an SPP of $\ell = -6$. (b) Direct imaging the OAM states through scattering media before algorithm optimization. (c) During algorithm optimization, the light intensity of the target area is significantly enhanced. The red circles indicate the target area to be optimized marked by the calibration.

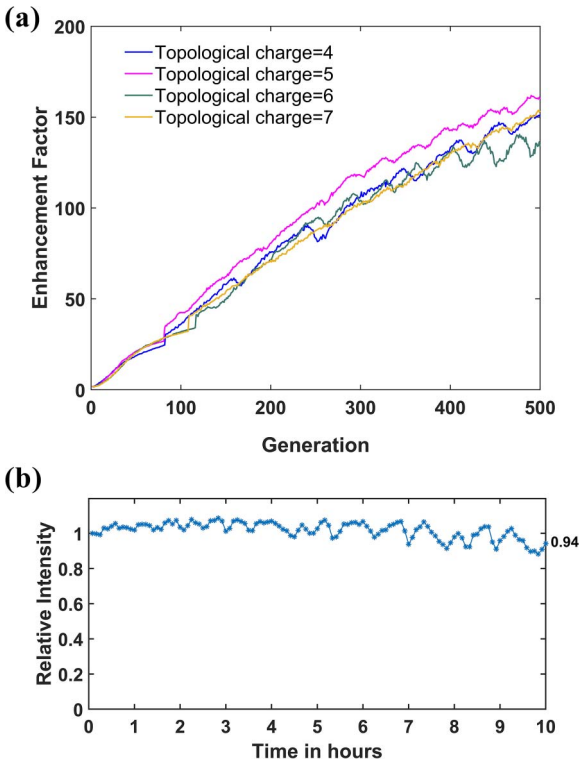

Fig. 5. (a) Enhancement factor curves of different topological charges ($\ell = 4 - 7$). In our experiment, a typical value is 150 after 500 generations. (b) Stability measurement of the focusing relative intensity over 10 h.

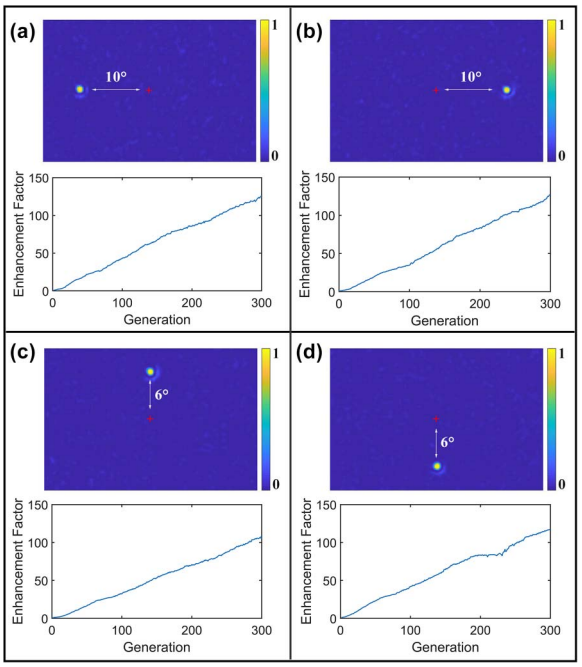

Fig. 6. Reconstitution of OAMs in different spatial directions. (a) and (b) have a deflection angle of around ±10°, while (c) and (d) have a pitch angle of around ±6°. The red cross is the optical axis direction of the original optical path.

the SLM, the optical axis orientation of the light path can be adjusted in a small range. The calibration and optimization processes are similar to the previous. Figure 6 shows the experiments on the reconstitution of the OAM beam with $\ell = 5$ at four different spatial directions, which corresponds to the deflection angle around ±10° and the pitch angle around ±6°, respectively. The evolution of the enhancement factor with the generation number is also shown in each figure. Without loss of generality, 300 generations are performed in our experiment, which can also achieve a relatively high enhancement. In fact, we can realize arbitrary direction manipulating OAM of light after the strong scattering medium theoretically, which will be more flexible and convenient when it is used in different fields. For example, alignment of the laser transmitting and receiving system is always needed at the process of optical communication. Therefore, our experiment provides a method to complete this task at the strong scattering environment.

4. Discussion

The main limit of the enhancement factor in our experiment comes from the modulation depth and degree of freedom of the SLM. In theory, more input modes will result in a higher enhancement[32]. However, a more nuanced division also brings greater complexity and time costs, which requires higher stability of the whole system. The problem may be improved by more accurate and quickly responsive modulation equipment, like a digital mirror device (DMD)[44–46]. In the experiment, only SPP was used to detect OAM after the scattering medium. Besides, it is possible to restore the multiplex OAM states by using another SLM to generate a hologram as a detection unit. Similarly, if the detection unit is replaced with a forked grating, it can realize the simultaneous restoration of multiple OAM states at different diffraction orders in space. The Laguerre–Gauss beam can also be generated after the scattering medium by measuring the transmission matrix[31]. In comparison, the advantages of the genetic algorithm are that it has better anti-interference ability and larger enhancement factor[32]. It is because the transmission matrix method requires that all measurements be made before the input pattern is calculated according to the target, whereas algorithm optimization is a step-by-step process. Even if disturbed midway, previous individuals with better performance have been retained in the population. Our method not only provides the possibility for the application of OAM beams in complex environments, but also gives a perspective for the manipulation of scattered light fields. Combining the presented technique with other schemes for temporal[35,47], polarization[48], spectral control[49], and the scattering transmission matrix measurement[50,51], non-ballistic light in a strong scattering medium can be manipulated and utilized in a multi-dimensional manner.

In conclusion, we have reported the reconstitution of optical OAMs scattered by strong turbid media via the FBWS method. In our experiment, the SPP with an opposite topological charge is used to detect the OAM of scattered light. Using algorithms to address random scattering problems effectively avoids

mathematically complex operations. Combining the optimization algorithm, the optical OAM information can be effectively extracted and enhanced after the strong scattering process. The enhancement factor was estimated to be 150 after optimization of 500 generations. Meanwhile, we have verified the feasibility of this method for OAM reconstitution of different topological charges and different spatial directions. This method has been confirmed to have good repeatability and robustness. Our system is also proven to have high stability. Actually, the enhancement of the scattered OAM states is a localized effect in a particular direction by wavelet path selection and constructive interference. Nevertheless, it still demonstrates both a unique perspective and significant progress in random optics. Consequently, this work paves a way for the use of OAM beams in complex media for optical communication and deep imaging.

Acknowledgement

This work was supported in part by the National Natural Science Foundation of China (NSFC) (Nos. 11734011, 62022058, 12074252, and 12004245), the National Key R&D Program of China (Nos. 2017YFA0303701 and 2018YFA0306301), the Shanghai Municipal Science and Technology Major Project (No. 2019SHZDZX01), the Shanghai Rising-Star Program (No. 20QA1405400), and the Shandong Quancheng Scholarship (No. 00242019024).

References

1. L. Allen, M. W. Beijersbergen, R. J. Spreeuw, and J. P. Woerdman, "Orbital angular momentum of light and the transformation of Laguerre–Gaussian laser modes," Phys. Rev. A **45**, 8185 (1992).
2. S. S. Oemrawsingh, J. A. van Houwelingen, E. R. Eliel, J. P. Woerdman, E. J. Verstegen, J. G. Kloosterboer, and G. W. t Hooft, "Production and characterization of spiral phase plates for optical wavelengths," Appl. Opt. **43**, 688 (2004).
3. N. R. Heckenberg, R. McDuff, C. P. Smith, and A. G. White, "Generation of optical phase singularities by computer-generated holograms," Opt. Lett. **17**, 221 (1992).
4. A. M. Yao and M. J. Padgett, "Orbital angular momentum: origins, behavior and applications," Adv. Opt. Photon. **3**, 161 (2011).
5. J. Arlt, K. Dholakia, L. Allen, and M. J. Padgett, "The production of multiringed Laguerre–Gaussian modes by computer-generated holograms," J. Mod. Opt. **45**, 1231 (1998).
6. E. Karimi, B. Piccirillo, E. Nagali, L. Marrucci, and E. Santamato, "Efficient generation and sorting of orbital angular momentum eigenmodes of light by thermally tuned q-plates," Appl. Phys. Lett. **94** (2009).
7. G. C. G. Berkhout and M. W. Beijersbergen, "Method for probing the orbital angular momentum of optical vortices in electromagnetic waves from astronomical objects," Phys. Rev. Lett. **101**, 100801 (2008).
8. G. C. Berkhout, M. P. Lavery, J. Courtial, M. W. Beijersbergen, and M. J. Padgett, "Efficient sorting of orbital angular momentum states of light," Phys. Rev. Lett. **105**, 153601 (2010).
9. Y. Wang, X. Ma, M. Pu, X. Li, C. Huang, W. Pan, B. Zhao, J. Cui, and X. Luo, "Transfer of orbital angular momentum through sub-wavelength waveguides," Opt. Express **23**, 2857 (2015).
10. N. Bozinovic, Y. Yue, Y. Ren, M. Tur, P. Kristensen, H. Huang, A. E. Willner, and S. Ramachandran, "Terabit-scale orbital angular momentum mode division multiplexing in fibers," Science **340**, 1545 (2013).
11. Z. Liu, S. Yan, H. Liu, and X. Chen, "Superhigh-resolution recognition of optical vortex modes assisted by a deep-learning method," Phys. Rev. Lett. **123**, 183902 (2019).
12. N. B. Simpson, L. Allen, and M. J. Padgett, "Optical tweezers and optical spanners with Laguerre–Gaussian modes," J. Mod. Opt. **43**, 2485 (1996).
13. H. He, M. E. Friese, N. R. Heckenberg, and H. Rubinsztein-Dunlop, "Direct observation of transfer of angular momentum to absorptive particles from a laser beam with a phase singularity," Phys. Rev. Lett. **75**, 826 (1995).
14. K. Ladavac and D. G. Grier, "Microoptomechanical pumps assembled and driven by holographic optical vortex arrays," Opt. Express **12, 1144** (2004). 3
15. M. P. J. Lavery, F. C. Speirits, S. M. Barnett, and M. J. Padgett, "Detection of a spinning object using light's orbital angular momentum," Science **341**, 537 (2013).
16. A. Mair, A. Vaziri, G. Weihs, and A. Zeilinger, "Entanglement of the orbital angular momentum states of photons," Nature **412**, 313 (2001).
17. J. T. Barreiro, T.-C. Wei, and P. G. Kwiat, "Beating the channel capacity limit for linear photonic superdense coding," Nat. Phys. **4**, 282 (2008).
18. F. Tamburini, G. Anzolin, G. Umbriaco, A. Bianchini, and C. Barbieri, "Overcoming the Rayleigh criterion limit with optical vortices," Phys. Rev. Lett. **97**, 163903 (2006).
19. Z. Y. Zhou, Y. Li, D. S. Ding, W. Zhang, S. Shi, and B. S. Shi, "Optical vortex beam based optical fan for high-precision optical measurements and optical switching," Opt. Lett. **39**, 5098 (2014).
20. V. D'Ambrosio, N. Spagnolo, L. Del Re, S. Slussarenko, Y. Li, L. C. Kwek, L. Marrucci, S. P. Walborn, L. Aolita, and F. Sciarrino, "Photonic polarization gears for ultra-sensitive angular measurements," Nat. Commun. **4**, 2432 (2013).
21. D. Palacios, D. Rozas, and G. A. Swartzlander, Jr., "Observed scattering into a dark optical vortex core," Phys. Rev. Lett. **88**, 103902 (2002).
22. M. Luo, Q. Chen, L. Hua, and D. Zhao, "Propagation of stochastic electromagnetic vortex beams through the turbulent biological tissues," Phys. Lett. A **378**, 308 (2014).
23. L. Shi, L. Lindwasser, W. Wang, R. Alfano, and A. Rodriguez-Contreras, "Propagation of Gaussian and Laguerre–Gaussian vortex beams through mouse brain tissue," J. Biophoton. **10**, 1756 (2017).
24. W. B. Wang, R. Gozali, L. Shi, L. Lindwasser, and R. R. Alfano, "Deep transmission of Laguerre–Gaussian vortex beams through turbid scattering media," Opt. Lett. **41**, 2069 (2016).
25. R. Fickler, M. Ginoya, and R. W. Boyd, "Custom-tailored spatial mode sorting by controlled random scattering," Phys. Rev. B **95, 161108** (2017). 4
26. L. Tianying, L. Ang, Z. Xiaopei, L. He, W. Liping, H. Hailong, C. Ze, L. Xiaoping, and L. Haibin, "Analyzing OAM mode purity in optical fibers with CNN-based deep learning," Chin. Opt. Lett. **17**, 100603 (2019).
27. L. Chen, R. K. Singh, A. Dogariu, Z. Chen, and J. Pu, "Estimating topological charge of propagating vortex from single-shot non-imaged speckle," Chin. Opt. Lett. **19, 022603** (2021).
28. L. Gong, Q. Zhao, H. Zhang, X. Y. Hu, K. Huang, J. M. Yang, and Y. M. Li, "Optical orbital-angular-momentum-multiplexed data transmission under high scattering," Light Sci. Appl. **8**, 27 (2019).
29. I. M. Vellekoop and A. P. Mosk, "Focusing coherent light through opaque strongly scattering media," Opt. Lett. **32**, 2309 (2007).
30. I. M. Vellekoop and A. P. Mosk, "Phase control algorithms for focusing light through turbid media," Opt. Commun. **281**, 3071 (2008).
31. A. Boniface, M. Mounaix, B. Blochet, R. Piestun, and S. Gigan, "Transmission-matrix-based point-spread-function engineering through a complex medium," Optica **4, 54** (2017).
32. D. B. Conkey, A. N. Brown, A. M. Caravaca-Aguirre, and R. Piestun, "Genetic algorithm optimization for focusing through turbid media in noisy environments," Opt. Express **20**, 4840 (2012).
33. Y. Qiao, Y. Peng, Y. Zheng, F. Ye, and X. Chen, "Second-harmonic focusing by a nonlinear turbid medium via feedback-based wavefront shaping," Opt. Lett. **42**, 1895 (2017).
34. A. Daniel, L. Liberman, and Y. Silberberg, "Wavefront shaping for glare reduction," Optica **3, 1104** (2016).
35. M. Mounaix, D. Andreoli, H. Defienne, G. Volpe, O. Katz, S. Gresillon, and S. Gigan, "Spatiotemporal coherent control of light through a multiple scattering medium with the multispectral transmission matrix," Phys. Rev. Lett. **116**, 253901 (2016).
36. O. Katz, P. Heidmann, M. Fink, and S. Gigan, "Non-invasive single-shot imaging through scattering layers and around corners via speckle correlations," Nat. Photon. **8**, 784 (2014).

37. J. Bertolotti, E. G. van Putten, C. Blum, A. Lagendijk, W. L. Vos, and A. P. Mosk, "Non-invasive imaging through opaque scattering layers," Nature **491**, 232 (2012).
38. S. Yoon, M. Kim, M. Jang, Y. Choi, W. Choi, S. Kang, and W. Choi, "Deep optical imaging within complex scattering media," Nat. Rev. Phys. **2**, 141 (2020).
39. R. Horstmeyer, H. Ruan, and C. Yang, "Guidestar-assisted wavefront-shaping methods for focusing light into biological tissue," Nat. Photon. **9**, 563 (2015).
40. J. Jin, J. Luo, X. Zhang, H. Gao, X. Li, M. Pu, P. Gao, Z. Zhao, and X. Luo, "Generation and detection of orbital angular momentum via metasurface," Sci. Rep. **6**, 24286 (2016).
41. G. Gibson, J. Courtial, M. Padgett, M. Vasnetsov, V. Pas'ko, S. Barnett, and S. Franke-Arnold, "Free-space information transfer using light beams carrying orbital angular momentum," Opt. Express **12**, 5448 (2004).
42. R. Corey, M. Kissner, and P. Saulnier, "Coherent backscattering of light," Am. J. Phys. **63**, 560 (1995).
43. P. C. de Oliveira, A. E. Perkins, and N. M. Lawandy, "Coherent backscattering from high-gain scattering media," Opt. Lett. **21**, 1685 (1996).
44. K. Nam and J. H. Park, "Increasing the enhancement factor for DMD-based wavefront shaping," Opt. Lett. **45**, 3381 (2020).
45. A. P. Mosk, A. Lagendijk, G. Lerosey, and M. Fink, "Controlling waves in space and time for imaging and focusing in complex media," Nat. Photon. **6**, 283 (2012).
46. I. M. Vellekoop, "Feedback-based wavefront shaping," Opt. Express **23**, 12189 (2015).
47. O. Katz, E. Small, Y. Bromberg, and Y. Silberberg, "Focusing and compression of ultrashort pulses through scattering media," Nat. Photon. **5**, 372 (2011).
48. Y. Guan, O. Katz, E. Small, J. Zhou, and Y. Silberberg, "Polarization control of multiply scattered light through random media by wavefront shaping," Opt. Lett. **37**, 4663 (2012).
49. E. Small, O. Katz, Y. Guan, and Y. Silberberg, "Spectral control of broadband light through random media by wavefront shaping," Opt. Lett. **37**, 3429 (2012).
50. S. Popoff, G. Lerosey, M. Fink, A. C. Boccara, and S. Gigan, "Image transmission through an opaque material," Nat. Commun. **1**, 81 (2010).
51. S. M. Popoff, G. Lerosey, R. Carminati, M. Fink, A. C. Boccara, and S. Gigan, "Measuring the transmission matrix in optics: an approach to the study and control of light propagation in disordered media," Phys. Rev. Lett. **104**, 100601 (2010).